

Interaction Map Driven Cocrystallization of Ambrisentan: Structural and Biopharmaceutical Evaluation

Jamshed Haneef,* Datta Markad, and Renu Chadha

Cite This: <https://dx.doi.org/10.1021/acs.cgd.0c00427>

Read Online

ACCESS |



Metrics & More

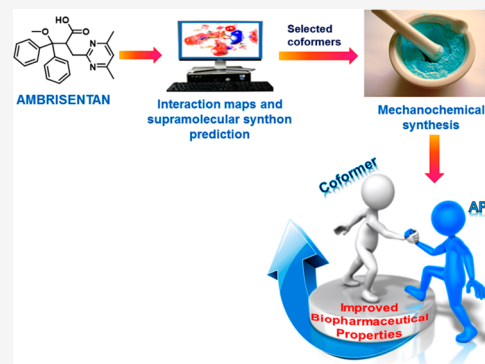


Article Recommendations



Supporting Information

ABSTRACT: The present work deals with the development of cocrystal of ambrisentan (AMT) to improve its biopharmaceutical profile. Full interaction maps (FIM) of AMT were explored to find out the potential sites for hydrogen bonding and prediction of supramolecular synthons. This information was further applied to the screening of amino acids as prospective cofomers for cocrystallization of AMT. Mechanochemical reactions have resulted in two cocrystals with L-aspartic acid and glycylglycine (dipeptide). The crystal structural analysis revealed that the hydrogen-bonding pattern in the developed cocrystals corroborated well with the predicted supramolecular synthons. The developed cocrystals showed a remarkable improvement in solubility, intrinsic dissolution rate, and *in vivo* systemic absorption as compared to the parent drug. Complementarily, Hirshfeld surface maps together with crystal features established a good structural–performance correlation of the developed cocrystals. Thus, the systematic cocrystallization driven by structural informatics tools is valuable in the development of novel solid forms with improved biopharmaceutical attributes.



1. INTRODUCTION

A major hurdle faced by the pharmaceutical industry in drug development is poor water solubility, which in turn impedes the bioavailability of new drug substances.¹ Most of these drugs belong to BCS II and IV classes, highlighting the challenging task before pharmaceutical scientists.² Therefore, there is a need to screen the potential solid-state form of a drug candidate with optimized physicochemical parameters for better bioavailability.^{3,4} The crystal engineering approach offers promising results in tailoring the biopharmaceutical properties of drugs.^{5,6} Cocrystallization is driven by supramolecular interaction among complementary functionalities that can be rationalized by synthons in the design of multicomponent solid forms.^{7–9} Pharmaceutical cocrystals have emerged as a viable route to optimize physicochemical (solubility, dissolution, stability),^{10,11} pharmacokinetic (bioavailability, permeability),^{12,13} and mechanical (flowability, compressibility, tableability)^{14,15} properties of challenging drug molecules. Additionally, the regulatory framework by the US-FDA considering a cocrystal as a new solid form of active pharmaceutical ingredients will further pull the interests of generic manufacturers toward the development of cocrystals.¹⁶

The prerequisite for the design of cocrystals is the proper understanding of supramolecular synthons or molecular recognition sites for the selection of suitable cofomers that are amenable to building molecular interaction. However, screening of a large array of cofomers requires several cocrystallization experimental trials, which is a time-consuming

process often resulting in few hits.¹⁷ Therefore, the selection of potential cofomers at a very early stage of cocrystal design would limit the experimental attempts, time, as well as cost. The Cambridge Structural Database (CSD) offers structural informatics tools for cocrystal design, prediction of cocrystal outcomes, and screening of potential cofomers.¹⁸ The various structural informatics tools employed are CSD intermolecular interaction search (ConQuest),¹⁹ hydrogen bond motif search,²⁰ hydrogen bonding propensity (HBP) prediction,²¹ and molecular complementarity.²² Besides, the full interaction map (FIM)²³ tool maps the entire molecule, reflecting the likelihood of supramolecular synthons by probing the functional groups, and is useful in the prediction of molecular crystal structures.

Ambrisentan (AMT) is an endothelin type A (ET_A) receptor blocker and is approved for the treatment of pulmonary arterial hypertension (PAH).²⁴ The poor water solubility (0.06 mg/mL) of AMT qualifies the drug to be categorized as BCS class II.²⁵ Form I of AMT is the only solid form which is approved for marketing under the brand name Letairis.²⁶ Our research group has explored this drug by developing its metastable solid

Received: March 28, 2020

Revised: June 5, 2020

Published: June 8, 2020

form (form II) and extensively studied its thermodynamic and surface anisotropic behavior.^{27,28} Besides, a solid dispersion of ambrisentan has also been reported²⁹ using a natural carrier to improve its bioavailability. However, amorphization of the resulting mixture together with an increase in bulk size further limits the translation to finished drug product. Therefore, the development of the multicomponent form based on the crystal engineering approach is a better alternative to improve the bioavailability of the selected drug. The availability of the pyrimidine ring and free carboxylic group in AMT further pulls our interest in developing cocrystals with complementary functional groups. Our recent study showed the propensity of AMT for cocrystallization with syringic acid (phenolic acid cofomer).³⁰ Motivated from the recent work, research was initiated to systematically explore other potential cofomers using crystal engineering and structural informatics tools.³¹ Current literature shows that the full interaction map (FIM) tool of CSD has been effectively used in the cocrystallization of drug molecules.^{32–34} The present attempt is focused on the application of FIM to identify functionalities capable of forming facile supramolecular synthons with recognition sites in the drug molecule. This information was further applied to the screening of amino acids as prospective cofomers for cocrystallization of AMT. The developed cocrystals were characterized using various analytical techniques. Besides, the structural–performance relationship has been derived from their physicochemical and biopharmaceutical properties.

2. EXPERIMENTAL SECTION

2.1. Materials. Ambrisentan (AMT) as form I was gifted by Dr Reddy's Laboratories, Hyderabad, India. Glycylglycine (GG, 99% purity) and L-aspartic acid (LAA, 99% purity) were procured from Himedia Laboratories Pvt. Ltd. (Mumbai, India) and used without any purification. All other chemicals and solvents were of analytical grade.

2.2. Preparation of the Cocrystals. The liquid-assisted grinding approach was used in the preparation of cocrystals in the presence of a catalytic amount of solvent. A stoichiometric amount of AMT (378.4 mg, 1 mmol) was ground separately with GG (132.1 mg; 1 mmol) and LAA (133.1 mg; 1 mmol) using an agate mortar and pestle with the addition of a few drops of ethanol, and ground for 30 min. The resulting solid mass was labeled AGG and ALAA, stored in a desiccator overnight, and characterized by various analytical tools.

2.3. Characterization Techniques. Differential scanning calorimetry (DSC) analyses of the samples were carried out using DSC Q20 (TA Instruments, New Castle, DE, USA) which was calibrated for temperature and heat flow accuracy using indium (mp 156.6 °C and ΔH of 25.45 J g⁻¹). Solid samples (4–6 mg) were placed in sealed nonhermetic aluminum pans and were scanned from 20 to 300 °C at 10 °C/min scanning rate under a dry nitrogen atmosphere (flow rate 50 mL/min). The data were analyzed using TA Instruments universal analysis 2000 software.

Powder X-ray diffraction (PXRD) of powder samples was recorded on the X'Pert PRO diffractometer system (PANalytical, Almelo, Netherlands) with a Cu K α radiation (1.54060 Å). The tube voltage and current were set at 45 kV and 40 mA, respectively. Diffraction pattern was measured by a continuous scan between 5° and 50° in 2θ with a step size of 0.017° and a step time of 25 s/step. Data was refined using X'Pert HighScore Plus software.

Fourier transform infrared (FTIR) spectra were recorded using Spectrum II (PerkinElmer, Waltham, MA, USA) in transmittance mode. Each spectrum was scanned in the range of 4000–400 cm⁻¹ with a resolution of 4 cm⁻¹, and a minimum of 16 scans was collected and averaged. Data were analyzed using Spectrum software.

¹³C-solid-state nuclear magnetic resonance (SSNMR) spectra were recorded on Jeol Resonance 400 MHz spectrometer (Jeol, Peabody,

Massachusetts, USA). SSNMR measurements were carried out on a 4 mm double resonance CP-MAS probe at 10 kHz spinning rate with a cross-polarization contact time of 3.5 ms and delay of 5 s using Delta NMR software.

2.4. Crystal Structure Determination from PXRD. BIOVIA Material Studio software (ver. 7.0) was used for the determination of the crystal structure of prepared cocrystal using the reflex plus module. The overall prediction process was carried out in four steps: indexing, Pawley fitting, structure solution, and Rietveld refinement. The optimized structure was further solved using Monte Carlo/simulated annealing procedure. Finally, Rietveld refinement of the structure solution was processed to obtain a final structure.³⁵

2.5. Hirshfeld Surface Analysis. Crystal Explorer 3.0 program was used to carry out Hirshfeld surface analysis (HSA) and generate fingerprint plots. The plots were used to describe various intermolecular interactions present in crystal structures of AGG, ALAA, and AMT. Crystallographic information files (CIFs) were used as input for the analysis. Directions and strengths of intermolecular interactions within the crystals were mapped onto the Hirshfeld surfaces using the descriptor " d_{norm} ", which is a ratio encompassing the distances of any surface point to the nearby interior (di) and exterior (de) atoms and the van der Waals radii of the atoms.²⁸

2.6. Physicochemical Evaluation. Apparent solubility was measured in 0.1 N HCl (pH 1.2) by suspending excess solid (cocrystal and parent drug) in 5 mL of media which is pre-equilibrated at 37 °C. The slurry obtained was shaken in a water bath shaker for 24 h. Samples were filtered through a 0.22 μm membrane filter and drug concentration was determined after appropriate dilution using the reported HPLC method.²⁷ The concentration of the sample was calculated from the calibration plot of the drug. Each experiment was repeated three times and average values were calculated.

Intrinsic dissolution study was carried out using a compressed disc of constant surface area (0.5 cm²) of powder samples (cocrystals and parent drug) on USP Dissolution apparatus (DS8000; LabIndia Analytical, Thane (West), Maharashtra, India). The compact disc was prepared using 100 mg powder sample with a hydraulic press at 55 MPa for 5 min and attached to a rotating disc holder. An intrinsic dissolution experiment was performed in a dissolution medium containing 500 mL of 0.1 N HCl (pH 1.2) preheated to 37.5 °C. The speed of the rotating disc holder was maintained at 150 rpm. Aliquots (5 mL) were withdrawn at a specified time interval, and concentration was determined from the calibration plot of AMT. The intrinsic dissolution rate (IDR) was calculated from linear regression analysis of the amount of drug dissolved per unit surface area of the compact disc for over 60 min.

2.7. In Vivo Pharmacokinetic Study. The animal study protocol was approved by the Institutional Animal Ethics Committee, Panjab University, Chandigarh, India (PU/IAES/S/14/77) following the Committee for the Purpose of Control and Supervision of Experiments on Animals (CPCSEA, 2015) guidelines for a laboratory animal. Male Wistar rats (~250 g) housed under standard laboratory conditions (25 \pm 2 °C and 55 \pm 5% relative humidity) with free access to standard diet and water. Animals were divided into three groups (AMT, AGG, and ALAA); each group consisted of four animals ($n = 5$). A single dose of all the samples equivalent to 2.5 mg kg⁻¹ body weight was suspended in 0.5% (w/v) sodium carboxymethylcellulose (CMC) and administered by oral gavage. Serial blood samples were collected from the retro-orbital venous plexus of the rats at 0 (predose), 0.5, 2, 4, 8, 12, 18, and 24 h into heparinized plastic tubes. The blood samples were then centrifuged at 10,000 rpm (1180g) for 10 min. The plasma was separated and treated with acetonitrile for protein precipitation. The treated plasma samples were stored at -20 °C until drug analysis was carried out by the reported HPLC method.²⁷ Pharmacokinetic parameters such as C_{max} , AUC_{0-12} , and relative bioavailability were calculated by using noncompartmental analysis employing Kinetica 5.0 (Thermo Scientific, Waltham, MA, USA).

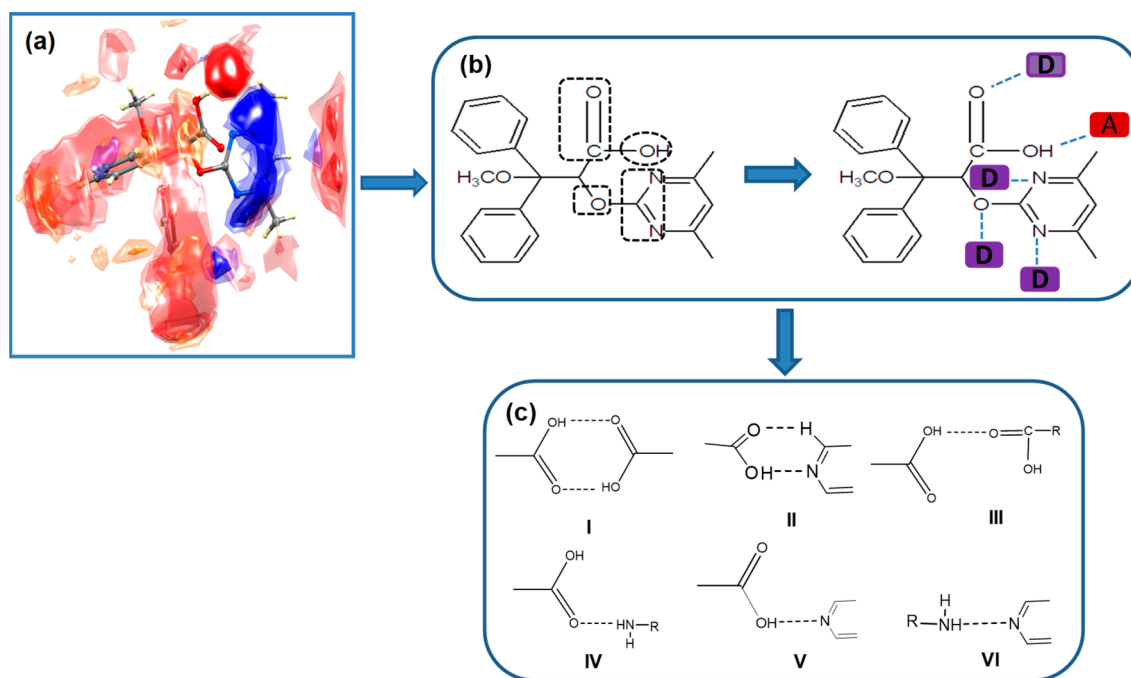


Figure 1. Full interaction map (FIM) around ambrisentan (form I). Regions of likely acceptor are shown in red, donors in blue, and hydrophobic groups in orange (a); Potential fragments in ambrisentan molecule for intermolecular interaction (D and A denotes likely hydrogen bond donor and acceptor, respectively, in another molecule) (b); Prediction of synthons (Types I–VI) based on FIM (c).

3. RESULTS AND DISCUSSION

3.1. Analysis of Full Interaction Maps (FIM) of Ambrisentan. FIM study was conducted to identify the active functional groups in the AMT molecule that are capable of potential interactions with another molecule. These interaction maps displayed the hydrogen bond acceptor and hydrogen bond donor sites around AMT that will help in the prediction of facile supramolecular synthons. These identified synthons between the drug molecule and surrounding sites will subsequently guide in the selection of suitable coformers for the cocrystallization. Figure 1a clearly shows the hot spot interaction regions (dark red contours, acceptor probe maps; and dark blue contours, donor probe maps), as well as some more transparent interaction regions (opaque red contours) around major fragments of the AMT. The interaction maps with dark contours (red/blue) suggest that these functionalities have high propensities for synthon formation, while transparent regions have lower propensities. Visual analysis of FIM of AMT shows that the hydroxyl of free carboxylic acid is surrounded by red hot spots indicating good sites for interaction with an acceptor group. Similarly, the carbonyl of free carboxylic acid, as well as the pyrimidine ring, is surrounded by blue hot spots suggesting interaction sites for a donor group. Interestingly, these interaction maps are very well correlated with the experimental crystal structure of polymorphic form I reported in the literature.³⁶ Form I showed a linear arrangement of AMT molecules and is sustained by hydrogen bonding interaction between OH_{acid} and pyrimidine nitrogen. However, in the reported crystal structures, the $\text{C}=\text{O}_{\text{acid}}$ group was not observed to satisfied the hydrogen bond donor preference maps which are seen in the FIM. The unsatisfied donor maps can be exploited by designing a cocrystal of AMT by selecting a suitable hydrogen bond donating coformer. Besides, many weak red contours have appeared around phenyl rings, although this region is free from

any potential hydrogen bond donor groups. However, some weakly activated C–H donors of phenyl hydrogen atoms can also participate in the interaction with suitable hydrogen bond accepting coformer.

3.2. Synthon Identification and Coformer Selection. FIM study provides the preferred sites (Figure 1b) that have high propensities to engage in hydrogen bond interaction with complementary functional groups in AMT. Based upon the observation of FIMs, the most suitable functional groups that may satisfy both donor and acceptor maps could be $-\text{OH}$, $-\text{NH}_2$, and $-\text{COOH}$. These functional groups may have the propensity to interact with complementary functionality in AMT and can be divided into six synthon networks (Figure 1c). Owing to the close presence of red and blue interaction maps around free carboxylic acid in AMT, it is speculative that both single and two-point interactions could be possible. Therefore, synthon types I and II have been identified showing two-point interaction between acid–acid and acid–pyrimidine. Besides, four different synthons (Types III, IV, V, and VI) have been identified, highlighting single point interaction with the preferred sites. Taking into account FIMs analysis and identified synthons, the complementary functionalities such as free carboxylic acid and amino groups may contribute to the development of cocrystal with AMT through one of the identifiable synthons.

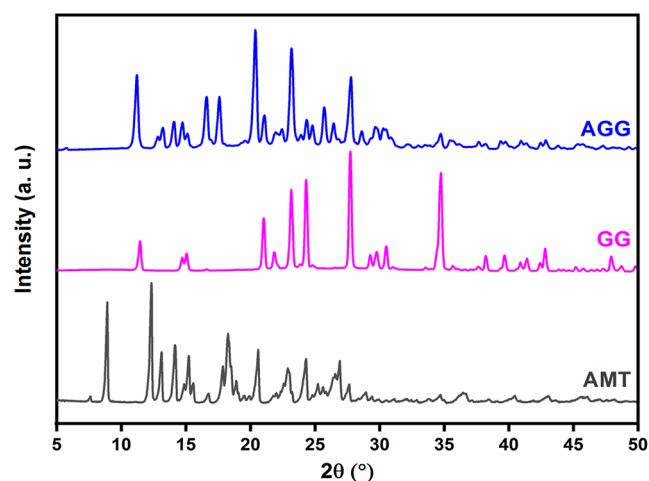
Amino acids seem to be a valuable choice as coformer because of their structural features (possessing both acidic and amide groups), good water solubility, low cost, and belonging to GRAS category. Amino acids have been extensively reported in the literature for the development of pharmaceutical cocrystals.³⁷ Therefore, nine different amino acids and one dipeptide (Table 1, Supporting Information) have been selected to drive the screening process for cocrystallization. The inclusion of the dipeptide (Glycylglycine) in the cocrystal screening was not a straightforward idea, but to compare the

Table 1. Crystallographic Parameters of Developed Cocrystals (AGG and ALAA)

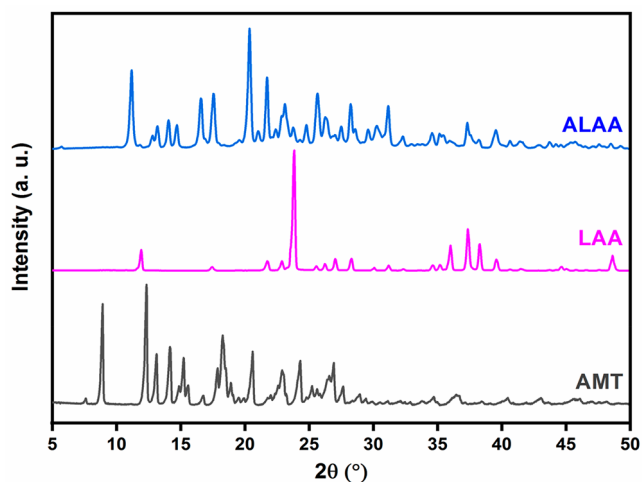
| parameters | AGG | ALAA |
|--------------------------|---|---|
| Molecular formula | C ₂₆ H ₃₀ N ₄ O ₇ | C ₂₆ H ₂₉ N ₃ O ₈ |
| Molecular weight | 510.54 | 511.52 |
| Crystal system | Monoclinic | Orthorhombic |
| Space group | <i>P2₁/a</i> | <i>Pcca</i> |
| <i>a</i> /Å | 25.3186 | 30.3484 |
| <i>b</i> /Å | 6.9860 | 24.2874 |
| <i>c</i> /Å | 14.2453 | 6.3241 |
| α /° | 90 | 90 |
| β /° | 107.6341 | 90 |
| γ /° | 90 | 90 |
| <i>V</i> /Å ³ | 2401.25 | 4661.39 |
| <i>Z</i> ' | 2 | 2 |
| 2θ range | 5–50° | 5–50° |
| CCDC deposition number | 1868627 | 1868620 |

outcomes with glycine only. The screening was conducted using a mechanochemical approach, preferably liquid assisted grinding (described in experimental section 2.2), and the ground product was characterized by various analytical tools.

3.3. Characterization of Cocrystals. PXRD is an important tool for the identification of new crystalline phases with distinct diffraction patterns.³⁸ PXRD patterns (Figure 2) of

**Figure 2.** Overlay of PXRD patterns of AMT, GG, and AGG cocrystal.

AGG reveal new signature peaks at 2θ values 16.6° and 17.6°, while the diffraction peaks of AMT and GG, respectively, at 8.9° and 34.7° disappeared. In the case of ALAA (Figure 3), new peaks appeared at 2θ values 11.1°, 16.5°, 17.5°, and 31.2°, while the prominent peak of AMT at 8.9° disappeared. Besides, some peaks of AMT at 24.3° and 22.9° were shifted, respectively, to 25.6° and 22.6° in ALAA. The emergence of distinct diffraction patterns of AGG and ALAA confirms the formation of the cocrystal. DSC curves provide good evidence for the phase purity of cocrystal.³⁹ DSC profile of AMT shows melting endotherm at 181 °C, while selected coformers, viz., GG and LAA shows endothermic events corresponding to their melting point at 241 and 239 °C, respectively (existence of adjacent endotherm is ascribed to polymorphic transformation). The liquid-assisted ground product of AGG and ALAA revealed a single melting endotherm at 220 and 215 °C,

**Figure 3.** Overlay of PXRD patterns of AMT, LAA, and ALAA cocrystal.

respectively (SI Figures 1 and 2). It is quite clear that the melting point of both ground products appeared in between the parent molecules as sharp and single peak indicating the existence of a homogeneous crystalline phase without any impurity of drug and coformers.

The molecular interaction between the cocrystal forming components has been explored by studying their vibrational spectra. The FTIR spectrum (SI, Figure 3) of AGG shows shifting in the C=O stretching band of AMT from 1752 to 1745 cm⁻¹. Similarly, carbonyl stretching band of GG at 1660 cm⁻¹ has shifted to 1662 cm⁻¹ in AGG. Moreover, the OH wagging in AMT and GG at 981 and 964 cm⁻¹ has also shifted to 998 cm⁻¹. This infers some form of interaction between carbonyl and OH_{acid} functionalities between drug and coformer. Additionally, the bending modes of NH₂ in GG show shifting from 1575 to 1545 cm⁻¹ indicating the involvement of free amino group also in hydrogen bonding in the resultant cocrystal. In the case of ALAA cocrystal, carbonyl stretching of AMT shifts from 1752 to 1745 cm⁻¹, while the bending vibration of C=N is shifted from 1559 to 1542 cm⁻¹ (SI, Figure 4). Besides, OH bending of LAA shifted from 1419 to 1425 cm⁻¹ in ALAA. The changes in the signature vibrational bands in ALAA are indicative of a possible interaction between complementary functionality, i.e., carbonyl of LAA and N_{arom} of AMT.

¹³C SSNMR offers valuable information on hydrogen bonding and is used as an important tool in understanding structural changes in multicomponent system.⁴⁰ ¹³C SSNMR spectrum of AGG showed some perturbation at the acidic C8 signal of AMT with a subtle shifting from 171 to 170 ppm, while a signal corresponding to acidic C1'(GG) was shifted from 174 to 173 ppm (SI, Figure 5). It is worth noting that the signal at 169 ppm corresponding to C1 (AMT) remain intact in AGG, which infers that the environment of N_{arom} was unaltered in the cocrystal. The above changes observed in the ¹³C SSNMR spectra are indicative of hydrogen bonding between corresponding acid functionalities among drug and coformer. Similarly, ¹³C SSNMR spectrum of ALAA (SI, Figure 6) showed a shift in signals of LAA from 176 ppm (C4') and 175 ppm (C1') to 175 and 174 ppm, respectively. Besides, subtle shifting was observed for the signal corresponding to C1 of AMT from 169 to 168 ppm in the resultant cocrystal. The above observation suggests the involvement of

pyrimidine nitrogen (N_{arom} adjacent to C1) in hydrogen bonding with OH of the carboxylic group (either C4' or C1'). Further, to understand which OH_{acid} is involved in the supramolecular interaction, the pattern of carbon signals was closely examined. In cocrystal, C1' signal noticeably merged toward the signal of C8 of AMT, while C4' appeared relatively sharp; therefore, it is anticipated that OH of C4' may be involved in the hydrogen bonding above. Additionally, a signal corresponding to C8 in AMT exhibits downfield shifting from 171 to 170 ppm with the bifurcation of the peak of equal intensity. This leads to the assumption that carboxylic acid (C8) may undergo dimer formation with another molecule. Further, it is reported⁴¹ that there is a higher chemical shift (180 ppm) after conversion of carboxylic acid to carboxylate form. It is interesting to mention that no signal at this region was noticed in the spectra of both cocrystals (AGG and ALAA), thus negating the assumption of salt formation.

3.4. Crystal Structure Determination from PXRD. The attempts to develop a single crystal of two developed cocrystals failed due to the incongruent solubility of drug and cofomers in the crystallizing solvents. Therefore, the crystal structure data of cocrystals were solved from their unique PXRD patterns. A good correlation exists between simulated and experimental powder diffraction patterns (SI, Figures 7 and 8). The crystallographic information on these cocrystals is summarized in Table 1. AGG crystal data reveals that the carbonyl of the carboxylic group in AMT interacts with OH_{acid} groups of GG as well as OH_{acid} of another AMT molecule, leading to bifurcated $\text{C}=\text{O}\cdots\text{HO}$ hydrogen bonds (synthons III) with a graph set (3) chain. This feature is very well correlated with the FIMs of AMT where dark blue contours were found near carbonyl of the acidic group and remain unsatisfied in the crystal structure of pure AMT (form I). Therefore, the success of the AGG cocrystal could be driven by synthons III acting as a primary structural unit. However, the bifurcate bonding of the carbonyl group is ascribed to the presence of lone pairs on the oxygen atom. Additionally, two inversion-related GG molecules form a dimer with a (16) ring motif through a $\text{NH}\cdots\text{O}$ network (synthons IV) between terminal secondary amine NH and carbonyl of carboxylic acid (Figure 4a). The GG dimer acting as a bridge to further propagate the hydrogen-bonded network with other AMT molecules thus acted as auxiliary interaction. It is quite evident that the crystal structure of AGG is sustained by two types of the supramolecular network via types III and IV synthons. The

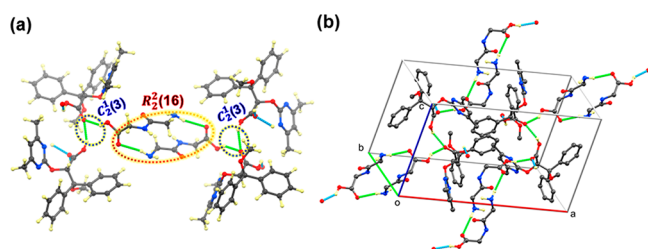


Figure 4. (a) Intermolecular interaction between AMT and GG molecules in cocrystal via supramolecular synthon network [bifurcated $\text{C}=\text{O}\cdots\text{OH}_{\text{acid}}$ (AMT)/ $\text{C}=\text{O}\cdots\text{OH}_{\text{acid}}$ (GG) and $\text{NH}\cdots\text{O}$ dimer]; (b) Packing diagram of the 3D supramolecular network formed by AMT and GG molecules in cocrystal via strong hydrogen bonds. Hydrogen bonds to carbon atoms are hidden to improve clarity. Expanded and hanging hydrogen-bonded contacts are represented in dotted green and cyan color, respectively.

packing structure of AGG showing a 3D supramolecular assembly of AMT and GG molecules via strong hydrogen bonding (Figure 4b).

The crystal structure of ALAA shows that the carboxylic OH of LAA forms bifurcated hydrogen bonds—one with pyrimidine nitrogen of AMT via $\text{OH}\cdots N_{\text{arom}}$ interaction (synthon V) with a graph set (4) and another with an ether linkage of AMT via $\text{OH}\cdots\text{O}$ network. The existence of synthons V very well agrees with the calculated interaction maps where pyrimidine ring, as well as oxygen atom (ether linkage), were surrounded by dark blue contours (hydrogen bond donor maps). The availability of a free OH_{acid} group of the cofomer within the contours may effectively satisfy the interaction preferences leading to the bifurcation of the hydrogen bond. Besides, the availability of terminal carboxylic functional groups in both AMT and LAA follow a self-recognition pattern through the carboxylic acid dimeric interaction (synthon I) forming an (8) ring motif (Figure 5a). The cocrystallization of ALAA is driven by synthons V as a

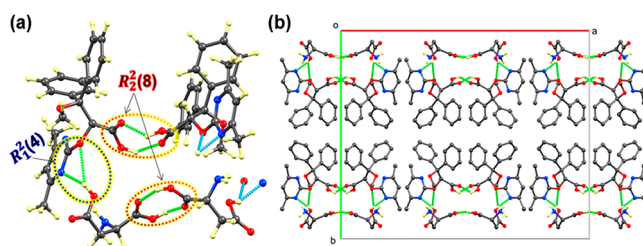


Figure 5. (a) Intermolecular interaction between AMT and LAA molecules in cocrystal via supramolecular synthon network [bifurcated $\text{OH}\cdots N_{\text{arom}}$ / $\text{OH}\cdots\text{O}$ and $\text{COOH}\cdots\text{COOH}$ dimer]; (b) Packing diagram of the 3D supramolecular network formed by AMT and LAA molecules in cocrystal via strong hydrogen bonds. Hydrogen bonds to carbon atoms are hidden to improve clarity. Expanded and hanging hydrogen-bonded contacts are represented in dotted green and cyan color, respectively.

primary structural unit, while synthons I are assumed to be an auxiliary interaction. It is interesting to mention that synthons V also exist in the crystal structure of AMT resulting in a dimeric interaction.³⁶ However, the formation of cocrystals has disrupted this homomeric AMT interaction, and a new heteromeric (drug–coformer) interaction is propagated by the bifurcated synthon network. The packing structure of ALAA shows a 3D supramolecular assembly of AMT and LAA molecules via strong hydrogen bonding (Figure 5b). It is worth mentioning that the synthon network observed in both cocrystals corroborated well with either one or more of the supramolecular synthons predicted by the FIM approach.

3.5. Structure–Performance Relationship of Developed Cocrystals. **3.5.1. Apparent Solubility and Structural Features Correlation.** Apparent solubility of cocrystals of AMT were measured in 0.1 N HCl at 37 °C for 24 h. AGG (0.65 ± 0.005 mg/mL) and ALAA (0.17 ± 0.006 mg/mL) show significant ($P > 0.001$) improvement in aqueous solubility as compared to pure AMT (0.07 ± 0.02 mg/mL). The correlation of physicochemical properties of a cocrystal with crystal structure features is difficult. Therefore, commonly used factors in these studies are cocrystal composition, cocrystal melting point, cofomer water solubility, and molecular features.^{42,43} The aqueous solubility experiment revealed that the developed cocrystal has improved solubility compared to pure AMT. By carefully examining the crystal

structure of the parent drug, it showed that there is a linear chain of homomeric synthon between carboxylic acid and pyrimidine nitrogen ($\text{OH}\cdots\text{N}_{\text{arom}}$) (SI, Figure 9). However, in AGG cocrystal, this primary synthon is absent, which may result in the improvement of its aqueous solubility. Conversely, ALAA cocrystal comprises $\text{OH}\cdots\text{N}_{\text{arom}}$ heterosynthon, similar to the parent drug, but bifurcated with an additional $\text{OH}\cdots\text{O}$ network, which may be ascribed to its higher solubility than the parent drug. It is also mentioned that the cofomer solubility also influences the solubility of the corresponding cocrystal.^{44,45} It is found that the aqueous solubility of GG is relatively higher than the LAA, which may be responsible for imparting higher solubility to AGG as compared to ALAA. Overall, the modified synthon network together with hydrophilic cofomers may play a role in improving the aqueous solubility of both the cocrystals over the parent drug.

3.5.2. Intrinsic Dissolution Study and Hirshfeld Surface Analysis Correlation. Figure 6 depicts the intrinsic dissolution

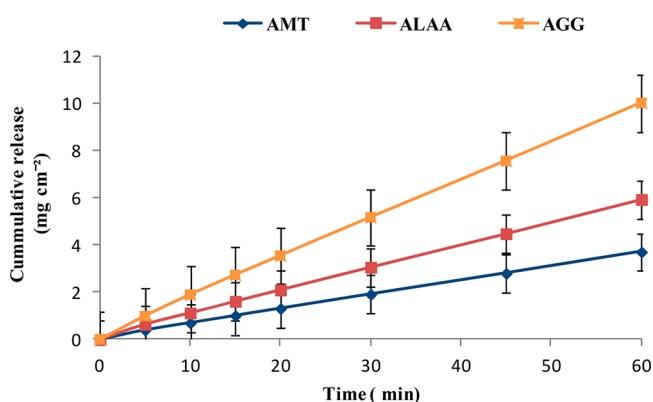


Figure 6. Intrinsic dissolution release profile of cocrystals (AGG and ALAA) and parent drug.

release profile of cocrystal of AMT in 0.1 N HCl (pH 1.2) dissolution medium at 37 °C. Among developed cocrystals, AGG showed higher IDR ($0.165 \pm 0.001 \text{ mg/cm}^2/\text{min}$) than ALAA ($0.097 \pm 0.001 \text{ mg/cm}^2/\text{min}$). The IDR of both cocrystals was found to be significantly higher ($P > 0.001$) than the pure AMT ($0.061 \pm 0.001 \text{ mg/cm}^2/\text{min}$). Up to 2.7-fold and 1.6-fold improvement in IDR of AGG and ALAA, respectively, was observed as compared to the parent drug. The significant improvement in dissolution rate in cocrystals is attributed to their better solubility. However, the dissolution is both a kinetic and surface phenomenon. Therefore, the factors responsible for solubility improvement may not be directly applicable to IDR. Hence, the surface molecular interaction in the developed cocrystals was mapped by studying their molecular Hirshfeld surface analysis (HSA) using Crystal Explorer. A plot of d_i versus d_e is a 2D fingerprint plots, which recognizes the existence of different types of intermolecular interactions and examine the local packing. 2D fingerprint plots of AMT and cocrystals were studied and found that among all the contacts, $\text{H}\cdots\text{H}$, $\text{C}\cdots\text{H}$, $\text{N}\cdots\text{H}$, and $\text{O}\cdots\text{H}$ were predominant. It is quite evident (Figure 7) that the polar interaction $\text{O}\cdots\text{H}$ is dominant in AGG (20.4%) over ALAA (16.2%) compared to AMT (14.2%), while $\text{N}\cdots\text{H}$ was found to be dominant in pure AMT (8.2%) as compared to developed cocrystals. Further, the percent contribution of nonpolar interaction, especially $\text{C}\cdots\text{H}$ in both cocrystals (ranges from 15–18%), was less than that in AMT (20.3%). Besides, in both cocrystals as well as AMT, the major contribution arises from the longer contacts $\text{H}\cdots\text{H}$ (53–57%). The above observation gives the correlation between polar surface contacts and IDR of developed cocrystals. The quantitative order of percent polar contacts in different solid forms $\text{AGG} > \text{ALAA} > \text{AMT}$ was found to be analogous to their dissolution release profile. It is anticipated that the presence of hydrophilic cofomers in the developed cocrystal contributes to the dominance of polar surface molecular environment, which are otherwise absent in the parent drug. On exposure to the aqueous medium, water-

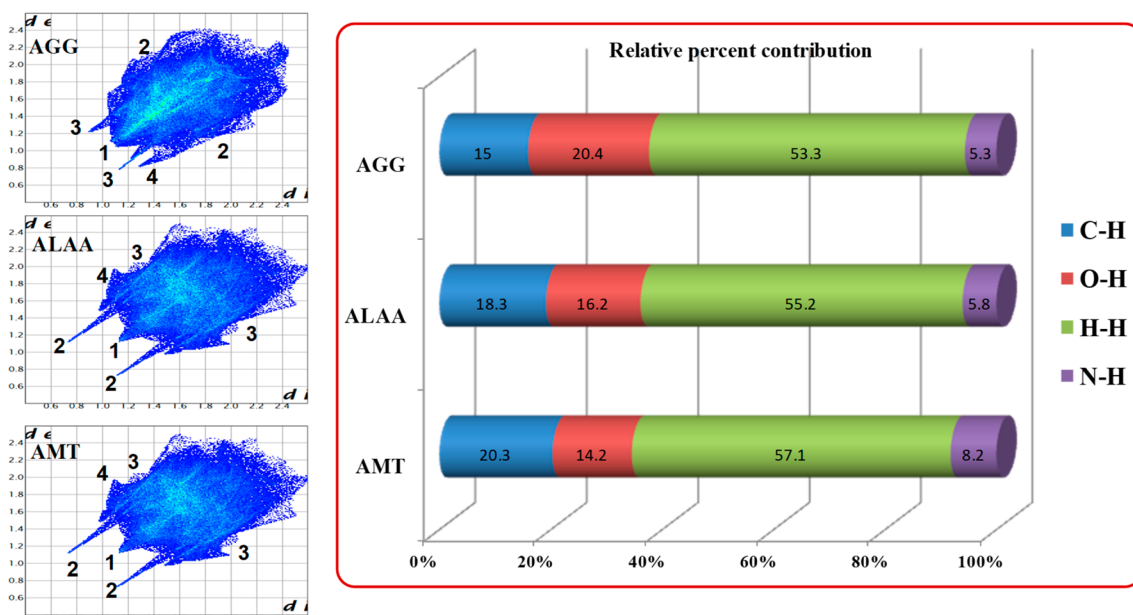


Figure 7. Left: 2D fingerprint plots derived from total Hirshfeld surface area for cocrystals and parent drug. Spikes labeled 1–4 represent the $\text{H}\cdots\text{H}$, $\text{N}\cdots\text{H}$, $\text{O}\cdots\text{H}$, and $\text{C}\cdots\text{H}$ interaction respectively. Right: Relative percent contribution of the intermolecular interactions to the Hirshfeld surface for cocrystals and parent drug.

soluble cofomers in cocrystals easily develop newer contacts with the solvent which facilitates solubilization of the cofomer molecules together with breaking of the crystal lattice. The remaining AMT molecules may form a transient amorphous aggregate which quickly solubilizes in the solution resulting in an enhanced dissolution rate.⁴⁶ The dissociation of cofomer from the cocrystal was quite evident from the PXRD study of IDR disc scrap after the experiment, which resembles the diffraction pattern of the parent drug (SI, Figures 10 and 11).

3.6. In Vivo Pharmacokinetic Study. Pharmacokinetic profiles of AMT and its cocrystals were determined by noncompartmental methods. Various pharmacokinetic parameters were determined using Kinetica software and are shown in Table 2. The developed cocrystals demonstrated superior

Table 2. Pharmacokinetic Parameters of Ambrisentan and Its Cocrystals

| drug/cocrystal ^a | C_{\max} ^b (ng mL ⁻¹) | AUC _{0–24} ^c (ng h mL ⁻¹) | Relative BA ^d |
|-----------------------------|--|---|--------------------------|
| AMT | 2518.08 | 21180.64 | - |
| AGG | 6829 | 42164.47 | 2 |
| ALAA | 3057.56 | 23428.16 | 1.1 |

^aAMT, ambrisentan; AGG, ambrisentan–glycylglycine cocrystal; ALAA, ambrisentan–L-aspartic acid cocrystal. ^bPeak of maximum concentration. ^cArea under the concentration–time profile curve until the last observation (up to 24 h). ^dRelative bioavailability of cocrystal with reference to the parent drug.

bioavailability owing to an increase in the extent of absorption (C_{\max} and AUC) and are depicted in Figure 8. Nearly 2-fold

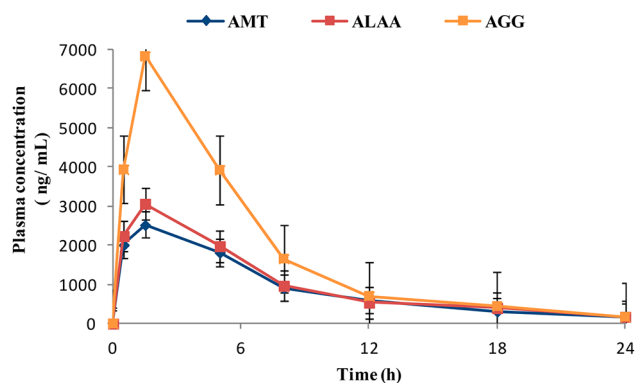


Figure 8. *In vivo* plasma concentration of ambrisentan at various time points in cocrystals, and parent drug. Values expressed in mean \pm SD ($n = 5$).

and 1.1-fold improvement in AUC were observed in AGG and ALAA, respectively, as compared to a parent drug suspension. Percent C_{\max} of developed cocrystals was in the range of 21–170% higher than the parent drug. This significant improvement can be attributed to the faster absorption of drug molecules in systemic circulation, which is ascribed to their high dissolution rate. Furthermore, improved pharmacokinetic profiles of developed cocrystals are found in good correlation with their *in vitro* dissolution study. Thus, the augmentation in the oral bioavailability of cocrystals is the interplay of their surface as well as structural features generated from drug–coformer interactions.

4. CONCLUSIONS

The present study highlights the successful attempt in the development of new cocrystals of AMT with amino acid (L-aspartic acid) and dipeptide (glycylglycine). The observed intermolecular interaction in cocrystals recognized the predicted supramolecular synthons through full interaction map approach. The developed cocrystals (AGG and ALAA) showed higher solubility and intrinsic dissolution rate as compared to the parent drug. The marked improvement in physicochemical properties of cocrystals was eloquently correlated with their structural features as well as the surface molecular environment using Hirshfeld surface analysis. This correlation suggested that the existence of supramolecular synthons and dominance of the polar molecular surface in cocrystals are responsible for their improved *in vitro* performance as compared to pure AMT. The advantage of better physicochemical properties in cocrystals translated into the overall augmentation of oral bioavailability in a pharmacokinetic study. It is important to mention that the FIM tool cannot mitigate the failure of cocrystallization despite having complementary functionality among cofomers. That is the reason many selected amino acids (except L-aspartic acid and dipeptide, glycylglycine) failed to give the cocrystal with drug molecule. It is believed that molecular size/shape complementarity and strength of cohesive and adhesive interaction may also be taken into consideration during the screening experiment. Besides, the ability of glycylglycine to generate cocrystal shows that deliberate efforts can be made to consider other small peptides in the cocrystallization screening for future endeavor.

ASSOCIATED CONTENT

Supporting Information

The Supporting Information is available free of charge at <https://pubs.acs.org/doi/10.1021/acs.cgd.0c00427>.

Cocrystallization screening of ambrisentan; DSC curves of AMT, GG, and AGG cocrystal; DSC curves of AMT, LAA, and ALAA cocrystal; Overlay of FTIR spectra of AMT, GG, and AGG; Overlay of FTIR spectra of AMT, LAA and ALAA; Overlay of ¹³C SSNMR spectra of AMT, GG, and AGG; Overlay of ¹³C SSNMR spectra of AMT, LAA, and ALAA; Rietveld plots of AGG and ALAA cocrystals; Homomeric synthon between carboxylic acid and pyrimidine nitrogen (OH \cdots Narom) in ambrisentan (form I); Overlay of PXRD patterns of cocrystals (AGG) and (ALAA) before and after solubility study (PDF)

Accession Codes

CCDC 1868620 and 1868627 contain the supplementary crystallographic data for this paper. These data can be obtained free of charge via www.ccdc.cam.ac.uk/data_request/cif, or by emailing data_request@ccdc.cam.ac.uk, or by contacting The Cambridge Crystallographic Data Centre, 12 Union Road, Cambridge CB2 1EZ, UK; fax: +44 1223 336033.

AUTHOR INFORMATION

Corresponding Author

Jamshed Haneef – Department of Pharmaceutical Chemistry, School of Pharmaceutical Education and Research, Jamia Hamdard, New Delhi 110 062, India; orcid.org/0000-0002-5520-6466; Phone: +91-8872082467; Email: jamshedhaneef@jamiahamdard.ac.in

Authors

Datta Markad – Department of Chemistry, University of Liverpool, Liverpool L69 7ZD, United Kingdom

Renu Chadha – University Institute of Pharmaceutical Sciences, UGC-Centre of Advanced Studies (CAS), Panjab University, Chandigarh 160 014, India

Complete contact information is available at:
<https://pubs.acs.org/10.1021/acs.cgd.0c00427>

Notes

The authors declare no competing financial interest.

ACKNOWLEDGMENTS

Authors are highly thankful for the services provided by the Sophisticated Analytical Instrumentation Facility (SAIF), Panjab University, India to carry out the analysis of the samples. Dr Jamshed Haneef greatly acknowledged the facility provided by the School of Pharmaceutical Education and Research, Jamia Hamdard, New Delhi.

REFERENCES

- (1) Thayer, A. M. Finding solutions—custom manufacturers take on drug solubility issue to help pharmaceutical firms move products through development. *Chem. Eng. News* **2010**, *88*, 13–18.
- (2) Kasim, N. A.; Whitehouse, M.; Ramachandran, C.; Bermejo, M.; Lennernas, H.; Hussain, A. S.; Junginger, H. E.; Stavchansky, S. A.; Midha, K. K.; Shah, V. P.; Amidon, G. L. Molecular properties of WHO essential drugs and provisional biopharmaceutical classification. *Mol. Pharmaceutics* **2004**, *1*, 85–96.
- (3) Aaltonen, J.; Allesø, M.; Mirza, S.; Koradia, V.; Gordon, K. C.; Rantanen, J. Solid form screening - A review. *Eur. J. Pharm. Biopharm.* **2009**, *71*, 23–37.
- (4) Gardner, C. R.; Walsh, C. T.; Almarsson, O. Drugs as materials: valuing physical form in drug discovery. *Nat. Rev. Drug Discovery* **2004**, *3*, 926–934.
- (5) Duggirala, N. K.; Perry, M. L.; Almarsson, O.; Zaworotko, M. J. Pharmaceutical cocrystals: along the path to improved medicines. *Chem. Commun.* **2016**, *52*, 640–655.
- (6) Bolla, G.; Nangia, A. Pharmaceutical cocrystals: walking the talk. *Chem. Commun.* **2016**, *52*, 8342–8360.
- (7) Almarsson, O.; Zaworotko, M. J. Crystal engineering of the composition of pharmaceutical phases. Do pharmaceutical co-crystals represent a new path to improved medicines? *Chem. Commun.* **2004**, *17*, 1889–1896.
- (8) Desiraju, G. R. Crystal engineering: a holistic view. *Angew. Chem., Int. Ed.* **2007**, *46*, 8342–8356.
- (9) Desiraju, G. R. Crystal Engineering: From Molecule to Crystal. *J. Am. Chem. Soc.* **2013**, *135*, 9952–9967.
- (10) Maheshwari, C.; Andre, V.; Reddy, S.; Roy, L.; Duarte, T.; Rodriguez-Hornedo, N. Tailoring aqueous solubility of a highly soluble compound via cocrystallization: effect of coformer ionization, pH_{max} and solute-solvent interactions. *CrystEngComm* **2012**, *14*, 4801–4811.
- (11) Elder, D. P.; Holm, R.; Diego, H. L. Use of pharmaceutical salts and cocrystals to address the issue of poor solubility. *Int. J. Pharm.* **2013**, *453*, 88–100.
- (12) Shaikh, R.; Singh, R.; Walker, G. M.; Croker, D. M. Pharmaceutical Cocrystal Drug Products: An Outlook on Product Development. *Trends Pharmacol. Sci.* **2018**, *39*, 1033–1048.
- (13) Shan, N.; Perry, M. L.; Weyna, D. R.; Zaworotko, M. J. Impact of pharmaceutical cocrystals: the effects on drug pharmacokinetics. *Expert Opin. Drug Metab. Toxicol.* **2014**, *10*, 1255–1271.
- (14) Halme, A.; Quayle, M. J.; Nilsson Lill, S. O.; Pettersen, A.; Fransson, M.; Boissier, C. Utilizing Crystal Structures for Predicting Impact of Mechanical and Surface Properties on Particle Fracture. *Cryst. Growth Des.* **2019**, *19*, 3670–3680.
- (15) Saha, S.; Mishra, M. K.; Reddy, C. M.; Desiraju, G. R. From Molecules to Interactions to Crystal Engineering: Mechanical Properties of Organic Solids. *Acc. Chem. Res.* **2018**, *51*, 2957–2967.
- (16) Kale, D. P.; Zode, S. S.; Bansal, A. K. Challenges in Translational Development of Pharmaceutical Cocrystals. *J. Pharm. Sci.* **2017**, *106*, 457–470.
- (17) Karimi-Jafari, M.; Padrela, L.; Walker, G. M.; Croker, D. M. Creating Cocrystals: A Review of Pharmaceutical Cocrystal Preparation Routes and Applications. *Cryst. Growth Des.* **2018**, *18*, 6370–6387.
- (18) Vologzhanina, A. V. Intermolecular Interactions in Functional Crystalline Materials: From Data to Knowledge. *Crystals* **2019**, *9*, 478.
- (19) Bilton, C.; Allen, F. H.; Shields, G. P.; Howard, J. A. K. Intramolecular hydrogen bonds: common motifs, probabilities of formation and implications for supramolecular organization. *Acta Crystallogr., Sect. B: Struct. Sci.* **2000**, *56*, 849–856.
- (20) Macrae, C. F.; Bruno, I. J.; Chisholm, J. A.; Edgington, P. R.; McCabe, P.; Pidcock, E.; Rodriguez-Monge, L.; Taylor, R.; van de Streek, J.; Wood, P. A. Mercury CSD 2.0 - new features for the visualization and investigation of crystal structures. *J. Appl. Crystallogr.* **2008**, *41*, 466–470.
- (21) Delori, A.; Galek, P. T. A.; Pidcock, E.; Patni, M.; Jones, W. Knowledge-based hydrogen bond prediction and the synthesis of salts and cocrystals of the anti-malarial drug pyrimethamine with various drug and GRAS molecules. *CrystEngComm* **2013**, *15*, 2916–2928.
- (22) Fabian, L. Cambridge Structural Database Analysis of Molecular Complementarity in Cocrystals. *Cryst. Growth Des.* **2009**, *9*, 1436–1443.
- (23) Wood, P. A.; Olsson, T. S. G.; Cole, J. C.; Cottrell, S. J.; Feeder, N.; Galek, P. T. A.; Groom, C. R.; Pidcock, E. Evaluation of molecular crystal structures using Full Interaction Maps. *CrystEngComm* **2013**, *15*, 65–72.
- (24) Croxtall, J. D.; Keam, S. J. Ambrisentan. *Drugs* **2008**, *68*, 2195–2204.
- (25) Assessment report for Volibris (INN:Ambrisentan). <http://www.emea.europa.eu> (1 May 2020).
- (26) Vizza, C. D.; Fedele, F.; Pezzuto, B.; Rubin, L. J. Safety and efficacy evaluation of ambrisentan in pulmonary hypertension. *Expert Opin. Drug Saf.* **2012**, *11*, 1003–1011.
- (27) Haneef, J.; Chadha, R.; Gupta, V.; Mandal, S. K. Novel polymorph of ambrisentan: Characterization and stability. *J. Pharm. Biomed. Anal.* **2018**, *153*, 102–109.
- (28) Haneef, J.; Chadha, R. Implication of Differential Surface Anisotropy on Biopharmaceutical Performance of Polymorphic Forms of Ambrisentan. *J. Pharm. Sci.* **2019**, *108*, 3792–3802.
- (29) Deshmene, S.; Shelke, S.; Biyani, K. Enhancement of solubility and bioavailability of ambrisentan by solid dispersion using *Daucus carota* as a drug carrier: formulation, characterization, in vitro, and in vivo study. *Drug Dev. Ind. Pharm.* **2018**, *44*, 1001–1011.
- (30) Haneef, J.; Chadha, R. Sustainable synthesis of ambrisentan - syringic acid cocrystal: Employing mechanochemistry in the development of novel pharmaceutical solid form. *CrystEngComm* **2020**, *22*, 2507–2516.
- (31) Wood, P. A.; Feeder, N.; Furlow, M.; Galek, P. T. A.; Groom, C. R.; Pidcock, E. Knowledge-based approaches to co-crystal design. *CrystEngComm* **2014**, *16*, 5839–5848.
- (32) Sandhu, B.; Sinha, A. S.; Desper, J.; Aakeroy, C. B. Modulating the physical properties of solid forms of urea using co-crystallization technology. *Chem. Commun.* **2018**, *54*, 4657–4660.
- (33) Wojnarska, J.; Gryl, M.; Seidler, T.; Stadnicka, K. M. Crystal engineering, optical properties and electron density distribution of polar multicomponent materials containing sulfanilamide. *CrystEngComm* **2018**, *20*, 3638–3646.
- (34) Kopczyńska, K.; Marek, P. H.; Banas, B.; Madura, I. D. Synthon preference in the cocrystal of 3,4,5-trifluorophenylboronic acid with urea. *Acta Crystallogr., Sect. C: Struct. Chem.* **2017**, *73*, 889–895.
- (35) Chadha, R.; Bhandari, S.; Haneef, J.; Khullar, S.; Mandal, S. Cocrystals of telmisartan: characterization, structure elucidation, in vivo and toxicity studies. *CrystEngComm* **2014**, *16*, 8375–8389.

- (36) Wei, Q. C.; Xu, H. Q.; Zhang, L. Y.; Wang, Y. L.; Tan, C. B.; Zhao, G. L. Synthesis and Crystal Structure of an Endothelin Receptor Antagonist Ambrisentan. *Chin. J. Struct. Chem.* **2013**, *32*, 1171–1174.
- (37) Tilborg, A.; Norberg, B.; Wouters, J. Pharmaceutical salts and cocrystals involving amino acids: a brief structural overview of the state-of-art. *Eur. J. Med. Chem.* **2014**, *74*, 411–426.
- (38) Thakral, N. K.; Zanon, R. L.; Kelly, R. C.; Thakral, S. Applications of Powder X-Ray Diffraction in Small Molecule Pharmaceuticals: Achievements and Aspirations. *J. Pharm. Sci.* **2018**, *107*, 2969–2982.
- (39) Detoisien, T.; Arnoux, M.; Taulelle, P.; Colson, D.; Klein, J. P.; Veessler, S. Thermal analysis: a further step in characterizing solid forms obtained by screening crystallization of an API. *Int. J. Pharm.* **2011**, *403*, 29–36.
- (40) Vogt, F. G.; Clawson, J. S.; Strohmeier, M.; Edwards, A. J.; Pham, T. N.; Watson, S. A. Solid-State NMR Analysis of Organic Cocrystals and Complexes. *Cryst. Growth Des.* **2009**, *9*, 921–937.
- (41) Gobetto, R.; Nervi, C.; Chierotti, M. R.; Braga, D.; Maini, L.; Grepioni, F.; Harris, R. K.; Hodgkinson, P. Hydrogen Bonding and Dynamic Behaviour in Crystals and Polymorphs of Dicarboxylic-Diamine Adducts: A Comparison between NMR Parameters and X-ray Diffraction Studies. *Chem. - Eur. J.* **2005**, *11*, 7461–7471.
- (42) Batisai, E.; Ayamine, A.; Kilinkissa, O. E. Y.; Bathori, N. B. Melting point-solubility-structure correlations in multicomponent crystals containing fumaric or adipic acid. *CrystEngComm* **2014**, *16*, 9992–9998.
- (43) Schultheiss, N.; Newman, A. Pharmaceutical Cocrystals and Their Physicochemical Properties. *Cryst. Growth Des.* **2009**, *9*, 2950–2967.
- (44) Aakeroy, C. B.; Forbes, S.; Desper, J. Using Cocrystals To Systematically Modulate Aqueous Solubility and Melting Behavior of an Anticancer Drug. *J. Am. Chem. Soc.* **2009**, *131*, 17048–17049.
- (45) Childs, S. L.; Chyall, L. J.; Dunlap, J. T.; Smolenskaya, V. N.; Stahly, B. C.; Stahly, G. P. Crystal Engineering Approach To Forming Cocrystals of Amine Hydrochlorides with Organic Acids. Molecular Complexes of Fluoxetine Hydrochloride with Benzoic, Succinic, and Fumaric Acids. *J. Am. Chem. Soc.* **2004**, *126*, 13335–13342.
- (46) Babu, N. J.; Nangia, A. Solubility Advantage of Amorphous Drugs and Pharmaceutical Cocrystals. *Cryst. Growth Des.* **2011**, *11*, 2662–2679.